

A Role for Melanopsin in Alpha Retinal Ganglion Cells and Contrast Detection

Tiffany M. Schmidt,^{1,*} Nazia M. Alam,² Shan Chen,³ Paulo Kofuji,⁴ Wei Li,³ Glen T. Prusky,² and Samer Hattar^{1,5}

¹Johns Hopkins University, Department of Biology, Baltimore, MD 21218, USA

²Department of Physiology and Biophysics, Weill Cornell Medical College, Burke Medical Research Institute, White Plains, NY 10605, USA

³National Eye Institute, National Institutes of Health, Bethesda, MD 20892, USA

⁴University of Minnesota, Department of Neuroscience, Minneapolis, MN 55455, USA

⁵Johns Hopkins University, Department of Neuroscience, Baltimore, MD 21218, USA

*Correspondence: tmschmidt@jhu.edu

<http://dx.doi.org/10.1016/j.neuron.2014.03.022>

SUMMARY

Distinct subclasses of retinal ganglion cells (RGCs) mediate vision and nonimage-forming functions such as circadian photoentrainment. This distinction stems from studies that ablated melanopsin-expressing intrinsically photosensitive RGCs (ipRGCs) and showed deficits in nonimage-forming behaviors, but not image vision. However, we show that the ON alpha RGC, a conventional RGC type, is intrinsically photosensitive in mammals. In addition to their classical response to fast changes in contrast through rod/cone signaling, melanopsin expression allows ON alpha RGCs to signal prior light exposure and environmental luminance over long periods of time. Consistent with the high contrast sensitivity of ON alpha RGCs, mice lacking either melanopsin or ON alpha RGCs have behavioral deficits in contrast sensitivity. These findings indicate a surprising role for melanopsin and ipRGCs in vision.

INTRODUCTION

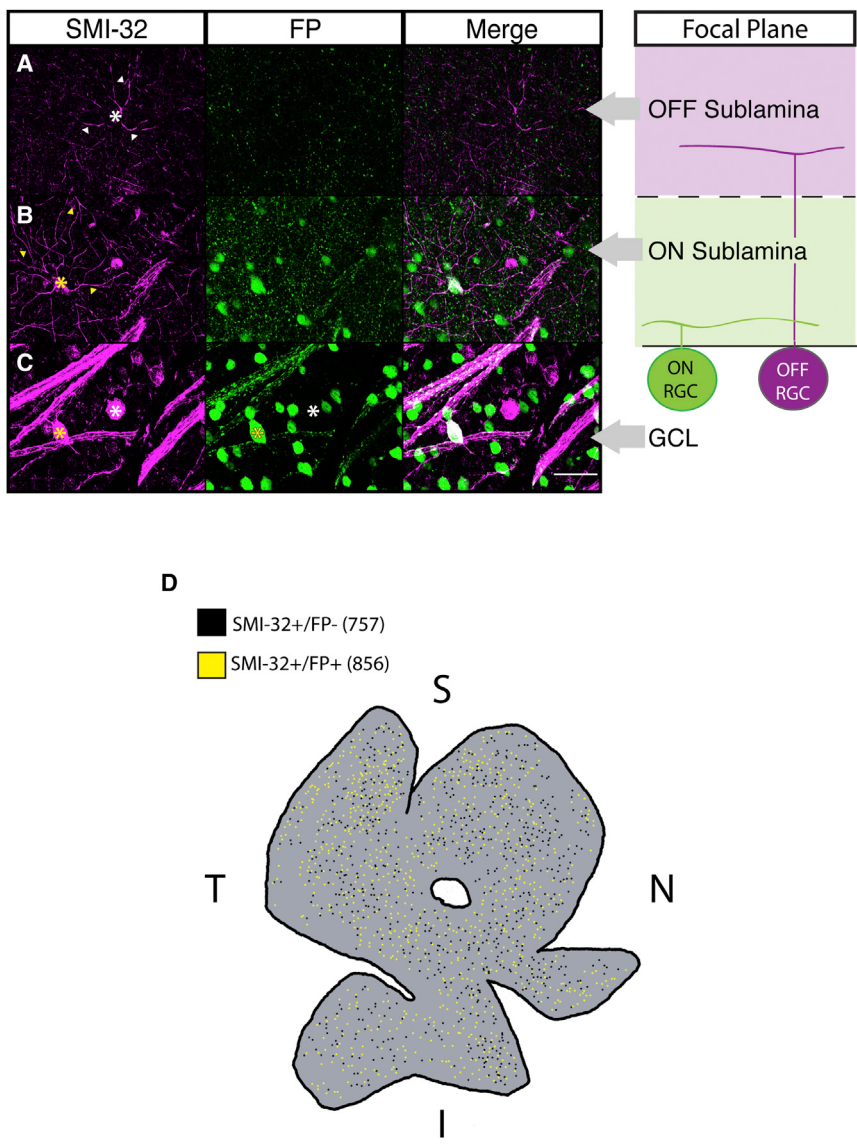
The visual system can be grossly divided into two systems: the image-forming visual system, which involves conscious perception of images, and the nonimage-forming visual system, which includes functions that occur outside of conscious awareness such as circadian photoentrainment and the pupillary light reflex. The image-forming visual system relies on rod and cone photoreceptors to detect light. These signals are then processed in the retina and relayed via conventional retinal ganglion cells (RGCs) to visual nuclei such as the dorsal lateral geniculate nucleus (dLGN) for further processing. The nonimage-forming visual system, however, relies almost exclusively on a distinct subset of RGCs that are intrinsically photosensitive RGCs (ipRGCs) and express melanopsin (Berson et al., 2002; Güler et al., 2008; Hattar et al., 2002). These photoreceptive neurons project to brain regions such as the suprachiasmatic nucleus (SCN), which mediates circadian photoentrainment, and the olfactory pretectal nucleus (OPN), which drives the pupillary light reflex (Hattar et al., 2006). Because genetic ablation of ipRGCs results in loss of nonimage-forming behaviors but retention of image-

forming vision via conventional RGCs, the logical assumption has been that RGCs driving nonimage- and image-forming behaviors are distinct (Güler et al., 2008). However, here we show that a well-described RGC type, the ON alpha (A-type) cell, characterized by large soma and dendritic field sizes (Boycott and Wässle, 1974), expresses melanopsin, is intrinsically photosensitive, and encodes irradiance over long periods. We also demonstrate that in ground squirrels the ON alpha-like RGCs, which have a transient rod/cone-driven response, are also intrinsically photosensitive. Moreover, mice lacking melanopsin (*Opn4*^{-/-}), or with ON alpha RGCs ablated (*Opn4*^{Cre/+}; *Brn3b*^{zDTA/+}; Chen et al., 2011), are defective in contrast detection, consistent with the demonstrated high contrast sensitivity of alpha RGCs (Enroth-Cugell and Robson, 1966; Shapley and Victor, 1978; Zaghloul et al., 2003). These findings reveal a functional role for melanopsin signaling in contrast detection in the presence of fully functional rod/cone signaling pathways.

RESULTS

ON Alpha RGCs Are Intrinsically Photosensitive

We found that a subset of fluorescently labeled ipRGCs (*Opn4*^{Cre/+}; *Brainbow-1.0* mice; Ecker et al., 2010; Livet et al., 2007) with large somas ($\geq 20 \mu\text{m}$) are immunopositive for the nonphosphorylated form of the neurofilament heavy chain protein (SMI-32; Figure 1C), which strongly labels alpha RGCs, in addition to weakly labeling other conventional RGC subtypes (Coombs et al., 2006; Lin et al., 2004). This is surprising because alpha cells project to image-forming brain regions and have high contrast sensitivity, which is essential for image formation. Alpha cells are divided into two populations that arborize in either the ON or OFF sublamina of the inner plexiform layer (IPL). These morphological divisions correlate with physiological responses to light increments (ON-center RGCs) or decrements (OFF-center RGCs) respectively (Famiglietti and Kolb, 1976; Kuffler, 1953). We found that only SMI-32-positive RGCs with dendrites stratifying in the ON sublamina expressed the melanopsin reporter (Figures 1B and 1C). Conversely, SMI-32-positive cells that stratified in the OFF sublamina were consistently negative for the fluorescent reporter (Figures 1A and 1C). However, we observed no colocalization when we immunostained for melanopsin and SMI-32, even with the most sensitive melanopsin antibody (Ecker et al., 2010; Provencio et al., 2002; Figure S1



available online), confirming previous reports (Coombs et al., 2006; Lin et al., 2004). These surprising results show that ON, but not OFF, alpha cells colabel with a melanopsin reporter.

Nearly half of SMI-32-labeled cells (n = 1,715/3,646 cells from N = 3 mice) were positive for the melanopsin fluorescent reporter in whole-mount retinas from *Opn4^{Cre/+};Brainbow-1.0* mice. The fluorescent protein-positive and -negative populations were distributed evenly throughout the retina (Figure 1D). Previously, five different subtypes of ipRGCs were identified by labeling with the *Opn4^{Cre}* reporter system on the basis of their morphological properties (Ecker et al., 2010). One distinctive subtype, M4, has been described as having “alpha-like morphology” and has the largest soma size of all ipRGC subtypes, dendrites that stratify in the ON sublamina, and does not stain with the most sensitive antibody against melanopsin unless amplification techniques are used (Figure S1; Coombs et al., 2006; Ecker et al., 2010; Estevez et al., 2012; Lin et al., 2004). As described above,

SMI-32-positive RGCs expressing the melanopsin reporter share all of these properties. This supports the hypothesis that ON alpha RGCs are the same cell population as those previously designated M4 ipRGCs.

Though it has been shown that M4 ipRGCs are “alpha-like” (Ecker et al., 2010; Estevez et al., 2012), it remains unclear whether all ON alpha RGCs are intrinsically photosensitive. To directly test this, we performed whole-cell recordings in wild-type (WT) retinas from putative alpha RGCs randomly selected based on soma size ($\geq 20 \mu\text{m}$; Pang et al., 2003). We encountered both ON-

and OFF-center alpha RGCs, which responded with a fast depolarization or hyperpolarization, respectively, to a 30 s bright, full-field 480 nm light stimulus (Figures 2B and 2H). After application of a cocktail of pharmacological agents to block synaptic transmission of rod and cone signals, ON (31/31; Figure 2C), but not OFF (0/8; Figure 2I), alpha RGCs responded intrinsically to light, showing that ON alpha RGCs are intrinsically photosensitive. We then filled each recorded cell with Neurobiotin and immunostained it for SMI-32. All recorded ON alpha RGCs were intrinsically photosensitive (n = 31; Figures 2A–2C), had large dendritic field diameter ($397.7 \pm 51.77 \mu\text{m}$, n = 8), large soma diameter ($31.47 \pm 3.73 \mu\text{m}$, n = 8), and were positive for SMI-32 (Figure 2A; Coombs et al., 2006; Lin et al., 2004). Importantly, ON RGCs that were not intrinsically photosensitive were SMI-32 negative (3/3) and had morphologies dissimilar to alpha RGCs. OFF alpha RGCs, in contrast, were all SMI-32 positive but none were intrinsically photosensitive (n = 8; Figure 2G).

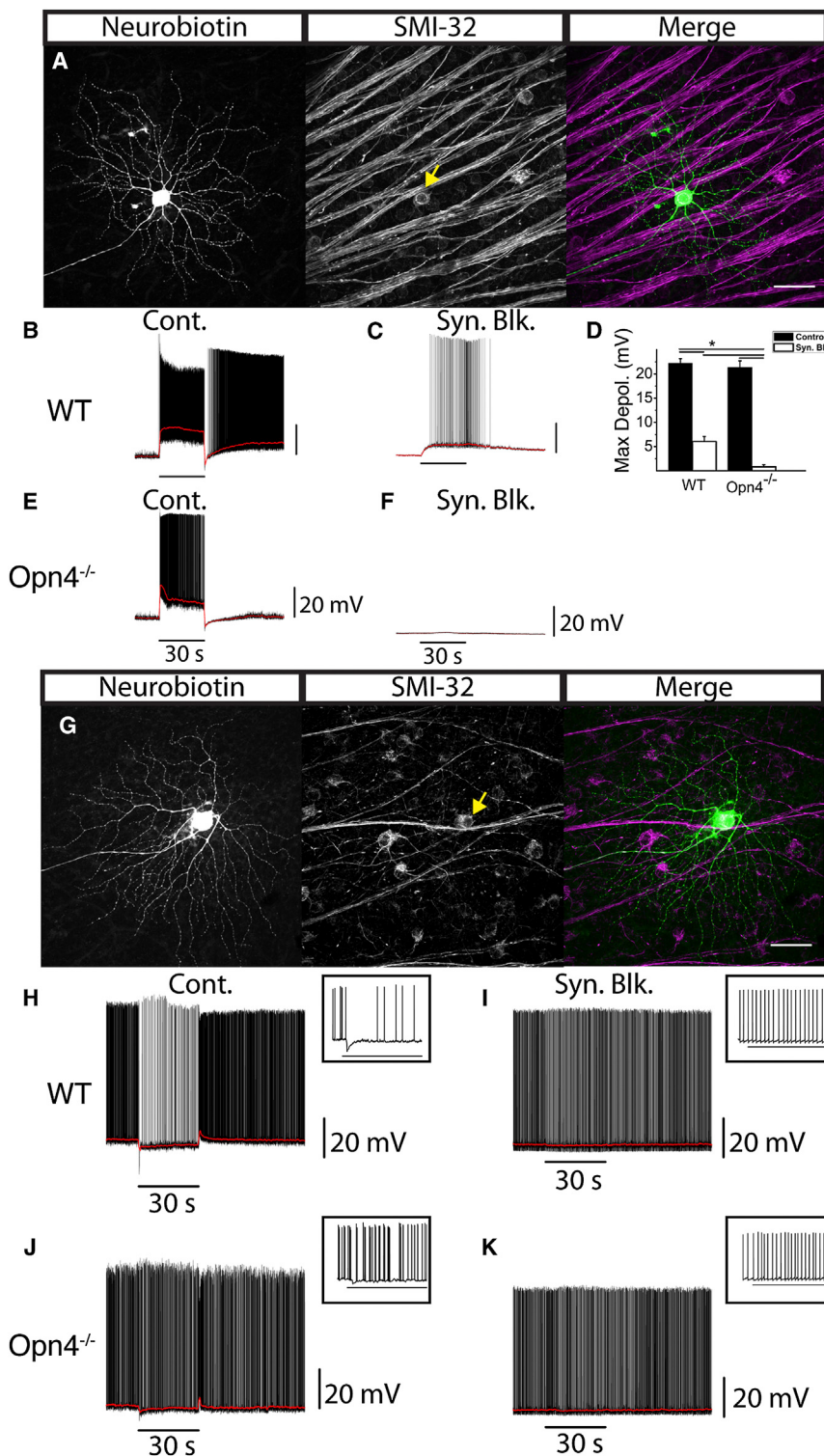


Figure 2. ON, but Not OFF, Alpha Cells Are Intrinsically Photosensitive

Cells with the largest soma sizes were randomly targeted for whole-cell recordings. (A) Cell recorded in (B) filled with Neurobiotin (left) and coimmunostained for SMI-32 (middle). Merged image (right) shows colocalization of Neurobiotin (green) and SMI-32 (magenta). (B) Whole-cell current-clamp recording of light response from ON alpha RGC in WT retina. (C) Cell from (B) recorded in the presence of a cocktail of synaptic blockers. (D) Mean \pm SEM maximum depolarization in ON alpha (SMI-32+) RGCs from WT ($n = 8$) and $Opn4^{-/-}$ ($n = 5$) mice under control conditions (black bars) and then in the presence of synaptic blockers (white bars). (E) Whole-cell current-clamp recording from ON alpha RGC in $Opn4^{-/-}$ retina. (F) Cell from (E) recorded in the presence of synaptic blockers. (G) Cell recorded from (H) filled with Neurobiotin (left) and coimmunostained for SMI-32 (middle). Merged image (right) shows colocalization of Neurobiotin (green) and SMI-32 (magenta). (H) Whole-cell current-clamp recording from OFF alpha RGC in a WT mouse. (I) Cell from (H) recorded in the presence of a cocktail of synaptic blockers. (J) Whole-cell current-clamp recording from OFF alpha RGC in $Opn4^{-/-}$ retina. (K) Cell from (J) recorded in the presence of synaptic blockers. Scale bars in (A) and (G), 50 μ m. (B–E and H–K) All cells were stimulated with 30 s, full-field, 480 nm stimulus. Horizontal bars indicate 30 s light stimulus. (H–K) Inset shows first ~3.5 s of response following light onset. * $p < 0.01$. RGC, retinal ganglion cell.

22.2 ± 0.9 mV $n = 8$, one-way ANOVA, $p < 0.01$; Figure 2D). Furthermore, their membrane potential remained elevated throughout the duration of the recording, even minutes after light offset, with only one out of eight cells decaying to 37% of maximum within the recording period. These properties implicate melanopsin-phototransduction in driving these intrinsic responses.

To test whether the intrinsic light responses of ON alpha RGCs is melanopsin dependent, we recorded from ON alpha RGCs in the retinas of $Opn4^{-/-}$ mice. Under control conditions, ON alpha RGCs in $Opn4^{-/-}$ mice responded to light (maximum depolarization = 21.3 ± 1.4 mV, $n = 5$) similarly to ON alpha cells in WT mice (maximum depolarization = 22.2 ± 0.9 mV, $n = 8$, one-way ANOVA,

The onset of light responses of ON alpha cells were significantly slower (change in 10%–90% RT = 18.9 ± 2.9 s, $n = 8$, t test, $p < 0.01$; Figure 2C) and smaller in the presence of synaptic blockers (maximum depolarization = 6.0 ± 1.1 mV, $n = 8$) compared to control conditions (maximum depolarization =

$p > 0.05$; Figures 2D and 2E). However, in contrast to the intrinsic response of WT mice (6.0 ± 1.1 mV, $n = 8$; Figure 2C), the light response of ON alpha RGCs was completely abolished in $Opn4^{-/-}$ mice upon application of synaptic blockers (0.8 ± 0.4 mV, $n = 5$, one-way ANOVA, $p < 0.01$; Figures 2D and 2F),

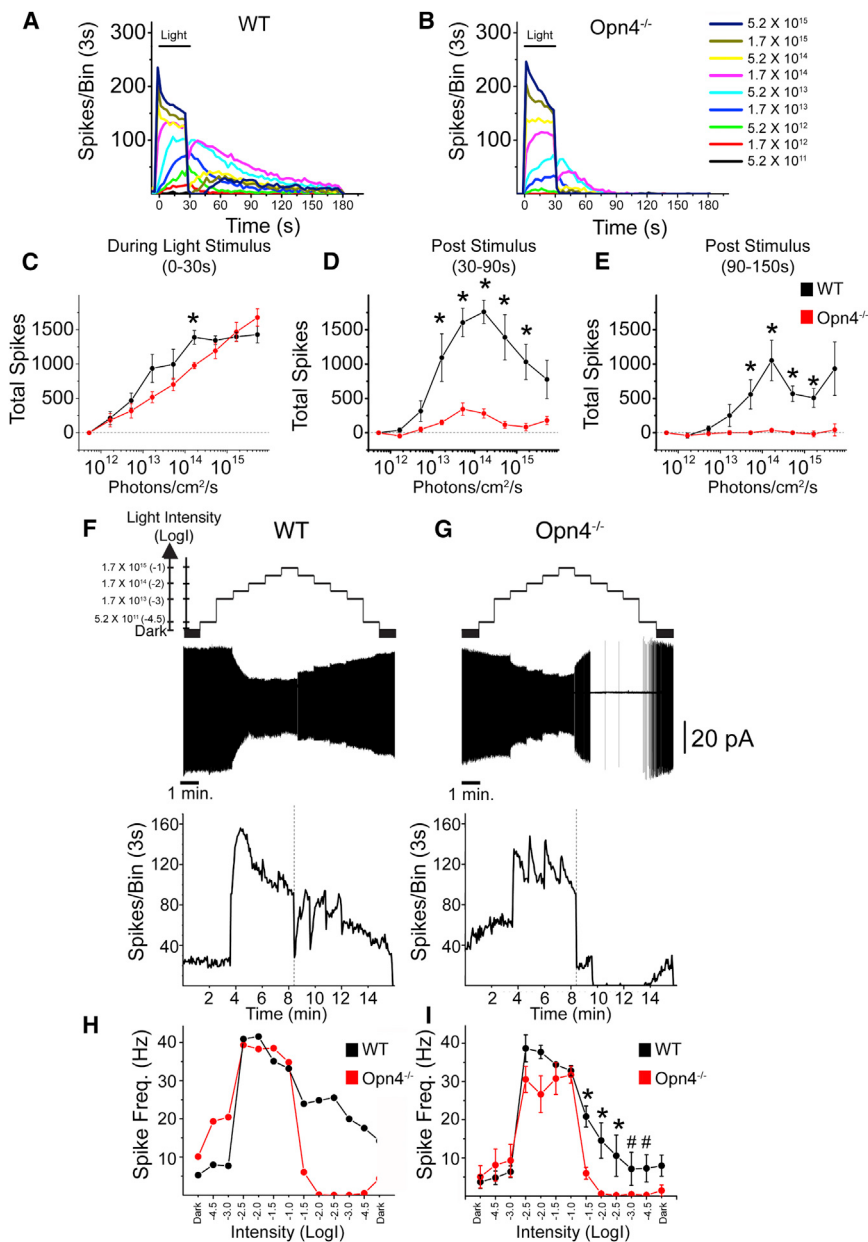


Figure 3. ON Alpha RGCs Signal Long-Term Lighting History and Irradiance

ON alpha RGCs of WT and *Opn4*^{-/-} mice were recorded extracellularly in loose-patch or cell-attached configuration. (A and B) Responses (spikes/3 s bin) of WT (A) and *Opn4*^{-/-} (B) ON alpha RGCs to increasing intensities of 480 nm light for 30 s (horizontal black bar) at various intensities. (C) Mean ± SEM total spikes recorded during 30 s light stimulus for ON alpha RGCs in WT (black, n = 4) and *Opn4*^{-/-} (red, n = 5) retinas. (D) Mean ± SEM total spikes of ON alpha RGCs recorded 0–60 s after light offset in WT (black) and *Opn4*^{-/-} (red) retinas. (E) Mean ± SEM total spikes of ON alpha RGCs recorded 60–120 s after light offset in WT (black) and *Opn4*^{-/-} (red) retinas. (F and G) ON alpha cells were exposed to 1 min steps of increasing and then decreasing irradiance from 5.2×10^{11} to 1.7×10^{15} photons/cm²/s. Top: representative examples of WT (F) and *Opn4*^{-/-} (G) ON alpha cells exposed to this light stimulus. Bottom: spikes/3 s bin of same WT (F) or *Opn4*^{-/-} (G) cells on the same timescale. Dotted line indicates point at which light intensities began to decrease. (H) Spike frequency for single WT (black) and *Opn4*^{-/-} (red) cells shown in (F) and (G) over 1 min at each light intensity (x axis = Log(intensity)). (I) Mean ± SEM spike frequency (Hz) for WT (black, n = 4) and *Opn4*^{-/-} (red, n = 4) ON alpha cells over 1 min at each light intensity (x axis = Log(intensity)). Horizontal scale bar in (F) and (G) represents 1 min of recording time and vertical scale bar (F) and (G) represents 20 pA. *p < 0.05, #p = 0.057 (Mann-Whitney U test).

showing that the intrinsic photosensitivity of ON alpha RGCs is melanopsin dependent. The synaptic response of OFF alpha RGCs in *Opn4*^{-/-} mice (n = 3) was similar to WT (Figures 2H and 2J), and no intrinsic response was detected in these cells (Figure 2K). Each recorded ON and OFF cell in *Opn4*^{-/-} mice was SMI-32 positive, indicating that we were sampling the same alpha RGC population in *Opn4*^{-/-} retinas as in WT.

The ON alpha cells of the mouse show sustained rod/cone-driven responses to light, which differ from the transient rod/cone-driven response of the classically identified cat ON alpha RGCs (Cleland and Levick, 1974). Therefore, we examined whether the ON alpha-like RGCs of the diurnal ground squirrel (*Ictidomys tridecemlineatus*), which has a functional melanopsin gene (Figure S2E; Provencio et al., 2000), are intrinsically photo-

sensitive. We randomly selected RGCs with the largest somas and confirmed ON alpha-like morphology, positive staining for SMI-32, and stratification in layer S4/S5 of the IPL by dye filling (Figures S2A–S2C and S2F; Linberg et al., 1996). ON alpha-like RGCs in squirrel responded to light with a transient inward current at light onset (Cleland et al., 1973; Jakiela and Enroth-Cugell, 1976; Figure S2D). Upon application of synaptic

blockers, we found that ON alpha-like RGCs had a sluggish and sustained inward current resembling a melanopsin-mediated light response (Figure S2E; n = 4), which persisted throughout the duration of the 30 s light stimulus and recovered slowly after stimulus offset (Figure S2E; n = 4). This indicates that the intrinsic photosensitivity of ON alpha-like RGCs exists in a diurnal mammal with a cone-dominated retina and may thus be found across a variety of species.

Melanopsin Influences ON Alpha RGC Signaling

To determine whether the intrinsic, melanopsin-based photoresponse contributes physiologically to ON alpha RGC signaling, we compared responses of ON alpha RGCs of WT and *Opn4*^{-/-} mice to 30 s stimuli of increasing irradiance (Figures 3A and 3B;

Figure S3). In WT and *Opn4*^{-/-} mice, ON alpha RGCs (n = 5 each) responded to increasing intensities of light with increasing spike frequencies during the 30 s light stimulus, reaching maximum average firing levels of >40 Hz (Figures 3A and 3C; Figure S3). However, a major difference between WT and *Opn4*^{-/-} animals was observed after cessation of the light stimulus. Four out of five ON alpha RGCs in WT mice showed continued elevation of spike frequencies after stimulus offset (Figure 3A; Figure S3) and were utilized for subsequent analyses. We found that the total number of spikes in the first 60 s after stimulus offset in WT ON alpha RGCs was intensity dependent (Figures 3A and 3D), reaching maximum spike output at 1.7×10^{14} photons/cm²/s (Figure 3D). In contrast, cells in *Opn4*^{-/-} mice showed markedly reduced levels of firing during this same period, though cells still showed slight increases in spike output between 5.2×10^{12} and 5.2×10^{13} photons/cm²/s (Figures 3B and 3D). A dramatic difference between ON alpha cell responses in WT and *Opn4*^{-/-} retinas was evident when we quantified the total number of spikes between 60 and 120 s after stimulus offset. As stimulus intensity increased, ON alpha RGCs continued to show steadily increasing poststimulus firing levels through 1.7×10^{14} photons/cm²/s in WT mice (Figure 3E), while cells in *Opn4*^{-/-} mice showed no appreciable increases (Figure 3E). The fact that ON alpha cells signal irradiance even after the light stimulus has ceased enables ON alpha RGCs to keep a record of lighting history.

As melanopsin is implicated in signaling ambient light intensity, we next recorded spike output from ON alpha RGCs in WT and *Opn4*^{-/-} retinas as the intensity of a 480 nm background light was steadily increased and then decreased at 1 min intervals with no intervening dark (see *Supplemental Experimental Procedures*; Figures 3F and 3G; Barlow and Levick, 1969). We found that ON alpha RGCs in WT (n = 4) and *Opn4*^{-/-} (n = 4) mice responded to the onset of illumination increases and were able to maintain elevated firing levels throughout the light stimulation (Figures 3F and 3G). As the light intensity was stepped down, ON alpha RGCs in WT mice responded to decreases in luminance with a fast initial offset of spiking followed by a robust rebound in spiking that was maintained throughout the remainder of the light pulse (Figures 3F, 3H, and 3I). However, cells in *Opn4*^{-/-} mice demonstrated complete cessation of firing by the second light decrement step (Figures 3G–3I). This repression was maintained throughout steps of decreasing intensity, consistent with the characteristics of an ON center RGC. Thus, while rods and cones mediate the response to sustained increases in illumination, melanopsin-mediated phototransduction enables ON alpha RGCs to signal ambient environmental irradiance regardless of whether the intensity has been increased or decreased.

Melanopsin Is Required for Normal Sensitivity

The contribution of melanopsin to the responses of ON alpha RGCs, which have high contrast sensitivity (Enroth-Cugell and Robson, 1966; Shapley and Victor, 1978; Zaghoul et al., 2003), raises the possibility that *Opn4*^{-/-} animals could have deficits in image-forming functions. We used optokinetic tracking (OKT; Douglas et al., 2005; Prusky et al., 2004) as an assay to measure contrast sensitivity and spatial frequency thresholds

in WT (N = 8) and *Opn4*^{-/-} (N = 8) animals (Figures 4A and 4B). Consistent with a role for melanopsin in alpha cell signaling, *Opn4*^{-/-} mice showed deficits in contrast sensitivity when compared to WT mice (Figure 4A). These were observed at the peak of the contrast sensitivity curve (0.064 c/d; one-way ANOVA, p < 0.001), as well as spatial frequencies of 0.092 c/d (one-way ANOVA; p < 0.001), 0.103 c/d (one-way ANOVA; p < 0.001), and 0.192 c/d (one-way ANOVA; p < 0.01; Figure 4A). Reduced contrast sensitivity in *Opn4*^{-/-} animals was also observed at various spatial frequencies as screen luminance was decreased from 54 lux to 2 lux (p < 0.05; Figure 4B). Consistent with the behavioral contrast sensitivity deficits at low light intensities, we were able to record melanopsin-mediated responses at similar, low light intensities in ON alpha RGCs in the isolated, dark-adapted retina (5.2×10^{11} photons/cm²/s; n = 6/6 cells; Figure 4D). We also measured contrast sensitivity in control (n = 8) and *Opn4*^{-/-} (n = 5) mice in a visual cortex-dependent assay: the visual water task (VWT; Prusky and Douglas, 2004). At 0.089 c/d, *Opn4*^{-/-} mice showed a significant reduction in contrast sensitivity compared to control mice (Figure 4E; t test; p < 0.01), consistent with the OKT results. The reduction in visual function in *Opn4*^{-/-} mice was specific to contrast sensitivity because spatial frequency thresholds in WT and *Opn4*^{-/-} mice did not differ (one-way ANOVA, p > 0.05; Figure 4F; Güler et al., 2008). Importantly, these findings also demonstrate that RGCs (such as ON alpha RGCs or other ipRGCs) that do not project to the accessory optic system, which is necessary for OKT, are nonetheless capable of modulating the optokinetic reflex (Figures 4A–4C).

To delineate the role of ipRGC subtypes in contrast sensitivity, we examined whether the ablation of M1 ipRGCs caused further deficits in contrast sensitivity using the *Opn4*^{aDTA/aDTA} mice, which have normal ON alpha RGC distribution but lack M1 ipRGCs (Figure S4). *Opn4*^{aDTA/aDTA} mice showed normal spatial frequency thresholds (one-way ANOVA, p > 0.05) and no deficits in contrast sensitivity beyond those observed in *Opn4*^{-/-} animals (Figures 4C and 4F). It is therefore unlikely that the contrast sensitivity deficits observed in *Opn4*^{-/-} animals are due to changes in retinal dopamine release since M1 ipRGCs are the only subtype of ipRGC that form a plexus with the dopaminergic amacrine cells (Vugler et al., 2007).

ON Alpha RGC Deletion Causes Severe Deficits in Contrast Sensitivity

To determine the contribution of the intrinsically photosensitive ON alpha RGCs themselves to contrast sensitivity, we utilized animals in which ON alpha RGCs are ablated (*Opn4*^{Cre/+}; *Brn3b*^{zDTA/+}; Chen et al., 2011). We found that SMI-32-positive cells were reduced by approximately 50% in these animals and those remaining were predominantly OFF stratified (t test, p < 0.05; Figure S4 and data not shown). These animals also lack other non-M1 ipRGC subtypes as well as the M1 ipRGCs that project to the SCN (Chen et al., 2011). Importantly, the *Opn4*^{Cre/+}; *Brn3b*^{zDTA/+} animals, which exhibit normal circadian photoentrainment, contain 200 remaining M1 ipRGCs that arborize with dopaminergic amacrine cells and still contain melanopsin (Chen et al., 2011). *Opn4*^{Cre/+}; *Brn3b*^{zDTA/+} animals showed severe contrast sensitivity deficits beyond those

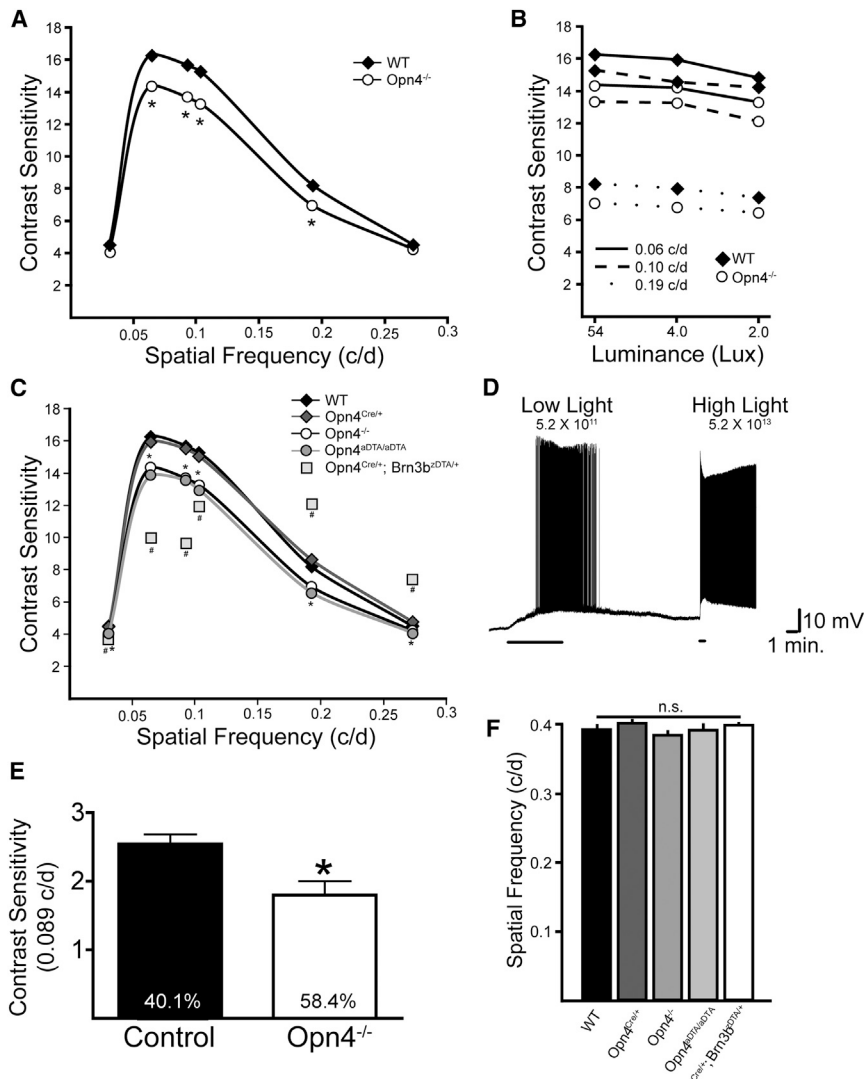


Figure 4. Melanopsin Phototransduction and Non-M1 ipRGCs Are Involved in Contrast Detection

(A) Contrast sensitivity plot of OKT response (each data point is average of both eyes; $N = 8$ mice) for WT and *Opn4^{-/-}* animals. (B) Reduced contrast sensitivity in *Opn4^{-/-}* mice relative to WT was maintained over a 25-fold decrease in luminance. **Opn4^{-/-}* mice showed significant deficits ($p < 0.05$; two-way ANOVA, Bonferroni post hoc test) in contrast sensitivity relative to WT at all spatial frequencies and luminances tested. (C) Contrast sensitivity plot of OKT response (each data point is average of both eyes; $N = 5$ –8 mice) for WT (replotted from A), *Opn4^{-/-}* (replotted from A), *Opn4^{Cre/+}*, *Opn4^{aDTA/aDTA}*, and *Opn4^{Cre/+}; Brn3b^{zDTA/+}* animals. **Opn4^{Cre/+}; Brn3b^{zDTA/+}* mice differ from WT at each spatial frequency but they do not differ from *Opn4^{-/-}* mice. #*Opn4^{Cre/+}; Brn3b^{zDTA/+}* animals differ from *Opn4^{Cre/+}* at all spatial frequencies and differ from *Opn4^{-/-}* mice at all spatial frequencies except the lowest (0.031; two-way ANOVA, Bonferroni post hoc test, significance concluded when $p < 0.05$). (D) Intrinsic light response of dark-adapted ON alpha RGC recorded in current-clamp mode in a cocktail of synaptic blockers for 5 min at dim light intensity comparable to the 2 lux stimulation used in (B) (5.2×10^{11} photons/cm²/s) and 30 s at bright light (5.2×10^{13} photons/cm²/s). Six out of six dark-adapted ON alpha RGCs showed intrinsic light responses at the low light intensities. (E) Contrast sensitivity measured in the VWT from control and *Opn4^{-/-}* mice at 0.089 c/d. The contrast threshold in percent contrast is denoted inside the bar for both genotypes. (F) WT, *Opn4^{-/-}*, *Opn4^{Cre/+}*, *Opn4^{aDTA/aDTA}*, and *Opn4^{Cre/+}; Brn3b^{zDTA/+}* animals do not differ in spatial frequency thresholds for OKT response (one-way ANOVA). “Contrast Sensitivity” is defined as $100 / [\% \text{ Contrast at Threshold Adjusted for Michelson Contrast}]$ (e.g., a threshold of 50% contrast would result in a contrast sensitivity of 2, see *Supplemental Experimental Procedures*). Data in all graphs are plotted as mean \pm SEM, but SEM is too small to visualize when plotted on this scale in (A)–(C). OKT, optokinetic tracking; VWT, visual water task.

observed in *Opn4^{-/-}* animals at the contrast sensitivity curve peak (0.064, 0.092, and 0.103 c/d; Figure 4C), indicating that non-M1 ipRGCs contribute to contrast sensitivity. As published previously, *Opn4^{Cre/+}; Brn3b^{zDTA/+}* animals show normal spatial frequency thresholds (one-way ANOVA, $p > 0.05$; Figure 4F; Chen et al., 2011), demonstrating the specificity of the non-M1 ipRGC contribution to contrast sensitivity. In addition, the number of choline acetyl transferase-positive amacrine cells in both the ganglion cell and inner nuclear layers was similar between *Opn4^{Cre/+}; Brn3b^{zDTA/+}* animals and control animals (Figure S4), indicating that these deficits are not due to defects in the direction selective circuitry. Interestingly, at higher spatial frequencies, *Opn4^{Cre/+}; Brn3b^{zDTA/+}* animals had enhanced contrast sensitivity (Figure 4C). The spatial frequencies where contrast sensitivity deficits were observed in *Opn4^{Cre/+}; Brn3b^{zDTA/+}* mice match the spatial frequencies over which

ON alpha RGCs respond to a sine wave grating stimulus in the isolated retina (Estevez et al., 2012), making it likely that the contrast sensitivity deficits in these animals arise as a result of ablation of the intrinsically photosensitive ON alpha RGCs.

DISCUSSION

ON alpha RGCs are intrinsically photosensitive and melanopsin signaling influences the physiological properties of these conventional RGCs. *Opn4^{-/-}* mice show defects in contrast sensitivity in both a subcortical optokinetic tracking task and a visual cortex-dependent task, providing a behavioral role for melanopsin in image-forming vision, even in the context of functional rods and cones. This decrease in contrast sensitivity in *Opn4^{-/-}* mice does not occur through M1 ipRGCs because ablation of M1 ipRGCs results in no further contrast sensitivity deficits beyond

those seen in melanopsin knockout animals. ON alpha RGCs were demonstrated to have high contrast sensitivity in vitro in other rodent models (Zaghoul et al., 2003), which suggests that melanopsin enhances behavioral contrast sensitivity at least in part through the ON alpha RGCs. Our data indicate that robust melanopsin responses can be driven in ON alpha RGCs at lower light intensities than previously appreciated, consistent with previous reports of melanopsin responses in ipRGCs at dim light (Wong, 2012) and consistent with a behavioral deficit in contrast sensitivity in mice lacking melanopsin at intensities of 2 lux (Figure 4B).

The severe contrast sensitivity deficits observed in mice where all non-M1 ipRGCs are ablated identify an important behavioral function for non-M1 ipRGCs and implicate this small population of ipRGCs in setting the thresholds for contrast detection. These results are consistent with recently identified non-M1 ipRGC connections to the dLGN in the mouse and primate (Dacey et al., 2005; Ecker et al., 2010; Estevez et al., 2012), as well as widespread melanopsin-derived light responses in 40% of light-sensitive neurons in the dLGN of mice (Brown et al., 2010). Collectively, these results show that melanopsin expression in non-M1 cells is not simply an evolutionary remnant but plays a crucial role in setting the threshold of contrast detection.

EXPERIMENTAL PROCEDURES

Animals

All animals were handled in accordance with guidelines of the Animal Care and Use Committees of Johns Hopkins University, the University of Minnesota, the National Eye Institute, or Cornell University. Specific details regarding strains used in each experiment as well as other methods can be found in the [Supplemental Experimental Procedures](#).

Electrophysiology

All electrophysiological analyses were performed as described previously (Schmidt and Kofuji, 2011; and see the [Supplemental Experimental Procedures](#)). Light stimulation was full-field band-pass filtered 480 nm light of 1.66×10^{16} photons/cm²/s for mouse retina recordings and 1.94×10^{16} photons/cm²/s for ground squirrel retina recordings.

Immunohistochemistry

Immunohistochemical studies were performed as described previously (Li and DeVries, 2004; Schmidt and Kofuji, 2009).

Statistical Analyses

Statistical analyses were performed using Origin 7.5 (MicroCal) or GraphPad Prism. Statistical comparison of means was performed using a Student's t test or one-way ANOVA with Tukey's post hoc test or a Mann-Whitney U test and significance was concluded when $p < 0.05$. Data are presented as mean \pm SEM.

Behavioral Analyses

Optokinetic tracking experiments were performed as described previously (Prusky et al., 2004; OptoMotry, CerebralMechanics). The visual water task was performed essentially as described previously (Prusky et al., 2000, 2004) but with printed instead of electronic grating stimuli.

SUPPLEMENTAL INFORMATION

Supplemental Information includes Supplemental Experimental Procedures and four figures and can be found with this article online at <http://dx.doi.org/10.1016/j.neuron.2014.03.022>.

ACKNOWLEDGMENTS

We would like to thank Drs. Marnie Halpern, Reiji Kuruvilla, Haiqing Zhao, Robert F. Miller, and Stewart Hendry for comments on the manuscript. We would also like to thank Dr. Cara Altimus, Ms. Diane Vig, and Mr. Nathan Schmidt for technical assistance. This work was funded by National Institutes of Health grants GM076430 (S.H.) and EY022543 (T.M.S.), the NIH Intramural Research Program (W.L.), and the Burke Foundation (G.T.P.). G.T.P. is a principal at Cerebral Mechanics, which manufactures equipment and software used in this study.

Accepted: February 26, 2014

Published: May 21, 2014

REFERENCES

- Barlow, H.B., and Levick, W.R. (1969). Changes in the maintained discharge with adaptation level in the cat retina. *J. Physiol.* 202, 699–718.
- Berson, D.M., Dunn, F.A., and Takao, M. (2002). Phototransduction by retinal ganglion cells that set the circadian clock. *Science* 295, 1070–1073.
- Boycott, B.B., and Wässle, H. (1974). The morphological types of ganglion cells of the domestic cat's retina. *J. Physiol.* 240, 397–419.
- Brown, T.M., Gias, C., Hatori, M., Keding, S.R., Semo, M., Coffey, P.J., Gigg, J., Piggins, H.D., Panda, S., and Lucas, R.J. (2010). Melanopsin contributions to irradiance coding in the thalamo-cortical visual system. *PLoS Biol.* 8, e1000558.
- Chen, S.K., Badea, T.C., and Hattar, S. (2011). Photoentrainment and pupillary light reflex are mediated by distinct populations of ipRGCs. *Nature* 476, 92–95.
- Cleland, B.G., and Levick, W.R. (1974). Brisk and sluggish concentrically organized ganglion cells in the cat's retina. *J. Physiol.* 240, 421–456.
- Cleland, B.G., Levick, W.R., and Sanderson, K.J. (1973). Properties of sustained and transient ganglion cells in the cat retina. *J. Physiol.* 228, 649–680.
- Coombs, J., van der List, D., Wang, G.Y., and Chalupa, L.M. (2006). Morphological properties of mouse retinal ganglion cells. *Neuroscience* 140, 123–136.
- Dacey, D.M., Liao, H.W., Peterson, B.B., Robinson, F.R., Smith, V.C., Pokorny, J., Yau, K.W., and Gamlin, P.D. (2005). Melanopsin-expressing ganglion cells in primate retina signal colour and irradiance and project to the LGN. *Nature* 433, 749–754.
- Douglas, R.M., Alam, N.M., Silver, B.D., McGill, T.J., Tscherter, W.W., and Prusky, G.T. (2005). Independent visual threshold measurements in the two eyes of freely moving rats and mice using a virtual-reality optokinetic system. *Vis. Neurosci.* 22, 677–684.
- Ecker, J.L., Dumitrescu, O.N., Wong, K.Y., Alam, N.M., Chen, S.K., LeGates, T., Renna, J.M., Prusky, G.T., Berson, D.M., and Hattar, S. (2010). Melanopsin-expressing retinal ganglion-cell photoreceptors: cellular diversity and role in pattern vision. *Neuron* 67, 49–60.
- Enroth-Cugell, C., and Robson, J.G. (1966). The contrast sensitivity of retinal ganglion cells of the cat. *J. Physiol.* 187, 517–552.
- Estevez, M.E., Fogerson, P.M., Ilardi, M.C., Borghuis, B.G., Chan, E., Weng, S., Auferkorte, O.N., Demb, J.B., and Berson, D.M. (2012). Form and function of the M4 cell, an intrinsically photosensitive retinal ganglion cell type contributing to geniculocortical vision. *J. Neurosci.* 32, 13608–13620.
- Famiglietti, E.V., Jr., and Kolb, H. (1976). Structural basis for ON-and OFF-center responses in retinal ganglion cells. *Science* 194, 193–195.
- Güler, A.D., Ecker, J.L., Lall, G.S., Haq, S., Altimus, C.M., Liao, H.W., Barnard, A.R., Cahill, H., Badea, T.C., Zhao, H., et al. (2008). Melanopsin cells are the principal conduits for rod-cone input to non-image-forming vision. *Nature* 453, 102–105.
- Hattar, S., Liao, H.W., Takao, M., Berson, D.M., and Yau, K.W. (2002). Melanopsin-containing retinal ganglion cells: architecture, projections, and intrinsic photosensitivity. *Science* 295, 1065–1070.

- Hattar, S., Kumar, M., Park, A., Tong, P., Tung, J., Yau, K.W., and Berson, D.M. (2006). Central projections of melanopsin-expressing retinal ganglion cells in the mouse. *J. Comp. Neurol.* 497, 326–349.
- Jakiela, H.G., and Enroth-Cugell, C. (1976). Adaptation and dynamics in X-cells and Y-cells of the cat retina. *Exp. Brain Res.* 24, 335–342.
- Kuffler, S.W. (1953). Discharge patterns and functional organization of mammalian retina. *J. Neurophysiol.* 16, 37–68.
- Li, W., and DeVries, S.H. (2004). Separate blue and green cone networks in the mammalian retina. *Nat. Neurosci.* 7, 751–756.
- Lin, B., Wang, S.W., and Masland, R.H. (2004). Retinal ganglion cell type, size, and spacing can be specified independent of homotypic dendritic contacts. *Neuron* 43, 475–485.
- Linberg, K.A., Suemune, S., and Fisher, S.K. (1996). Retinal neurons of the California ground squirrel, *Spermophilus beecheyi*: a Golgi study. *J. Comp. Neurol.* 365, 173–216.
- Livet, J., Weissman, T.A., Kang, H., Draft, R.W., Lu, J., Bennis, R.A., Sanes, J.R., and Lichtman, J.W. (2007). Transgenic strategies for combinatorial expression of fluorescent proteins in the nervous system. *Nature* 450, 56–62.
- Pang, J.J., Gao, F., and Wu, S.M. (2003). Light-evoked excitatory and inhibitory synaptic inputs to ON and OFF alpha ganglion cells in the mouse retina. *J. Neurosci.* 23, 6063–6073.
- Provencio, I., Rodriguez, I.R., Jiang, G., Hayes, W.P., Moreira, E.F., and Rollag, M.D. (2000). A novel human opsin in the inner retina. *J. Neurosci.* 20, 600–605.
- Provencio, I., Rollag, M.D., and Castrucci, A.M. (2002). Photoreceptive net in the mammalian retina. This mesh of cells may explain how some blind mice can still tell day from night. *Nature* 415, 493.
- Prusky, G.T., and Douglas, R.M. (2004). Characterization of mouse cortical spatial vision. *Vision Res.* 44, 3411–3418.
- Prusky, G.T., West, P.W., and Douglas, R.M. (2000). Behavioral assessment of visual acuity in mice and rats. *Vision Res.* 40, 2201–2209.
- Prusky, G.T., Alam, N.M., Beekman, S., and Douglas, R.M. (2004). Rapid quantification of adult and developing mouse spatial vision using a virtual optometer system. *Invest. Ophthalmol. Vis. Sci.* 45, 4611–4616.
- Schmidt, T.M., and Kofuji, P. (2009). Functional and morphological differences among intrinsically photosensitive retinal ganglion cells. *J. Neurosci.* 29, 476–482.
- Schmidt, T.M., and Kofuji, P. (2011). An isolated retinal preparation to record light response from genetically labeled retinal ganglion cells. *J. Vis. Exp.* Published online January 26, 2011. <http://dx.doi.org/10.3791/2367>.
- Shapley, R.M., and Victor, J.D. (1978). The effect of contrast on the transfer properties of cat retinal ganglion cells. *J. Physiol.* 285, 275–298.
- Vugler, A.A., Redgrave, P., Semo, M., Lawrence, J., Greenwood, J., and Coffey, P.J. (2007). Dopamine neurones form a discrete plexus with melanopsin cells in normal and degenerating retina. *Exp. Neurol.* 205, 26–35.
- Wong, K.Y. (2012). A retinal ganglion cell that can signal irradiance continuously for 10 hours. *J. Neurosci.* 32, 11478–11485.
- Zaghoul, K.A., Boahen, K., and Demb, J.B. (2003). Different circuits for ON and OFF retinal ganglion cells cause different contrast sensitivities. *J. Neurosci.* 23, 2645–2654.

Neuron, Volume 82

Supplemental Information

A Role for Melanopsin in Alpha Retinal Ganglion Cells and Contrast Detection

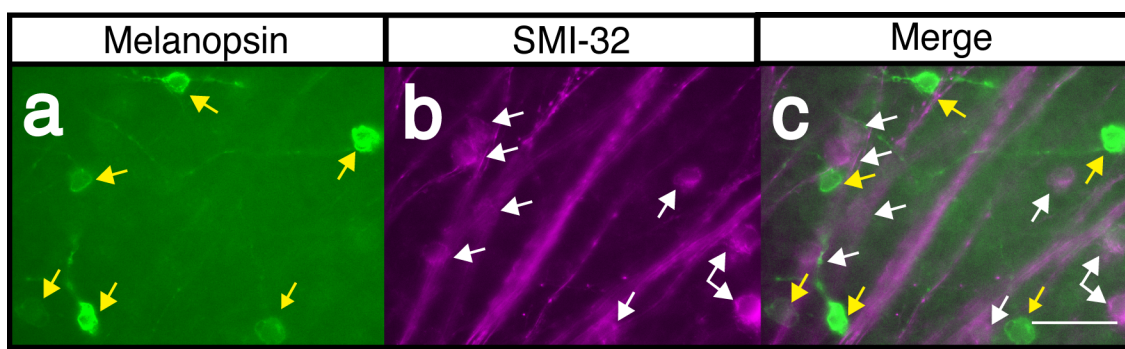
**Tiffany M. Schmidt, Nazia M. Alam, Shan Chen, Paulo Kofuji, Wei Li, Glen T. Prusky, and
Samer Hattar**

A role for melanopsin in alpha retinal ganglion cells and contrast detection

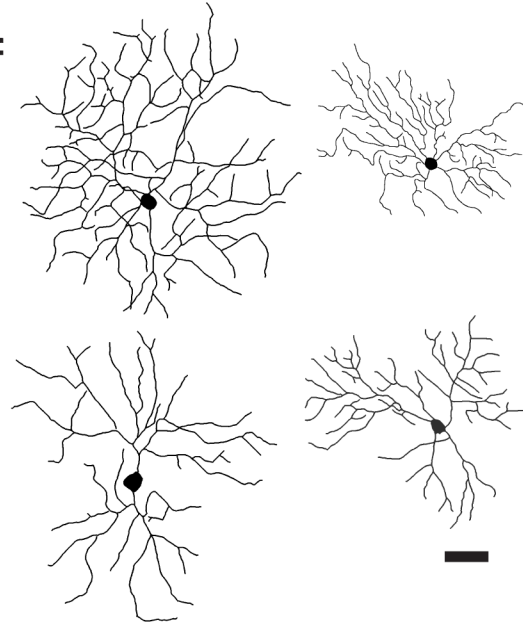
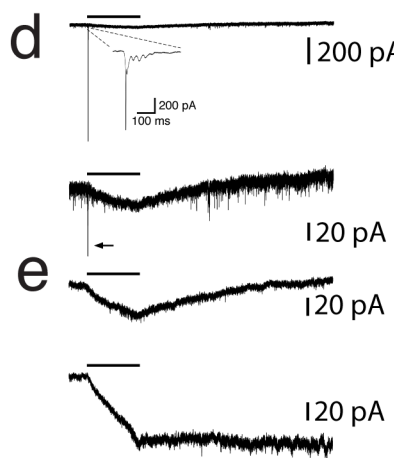
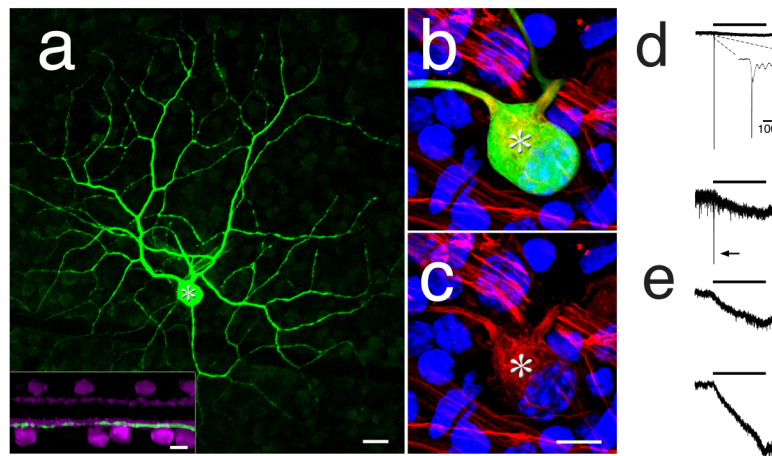
Schmidt et al.

Table of Contents for Supplementary Material

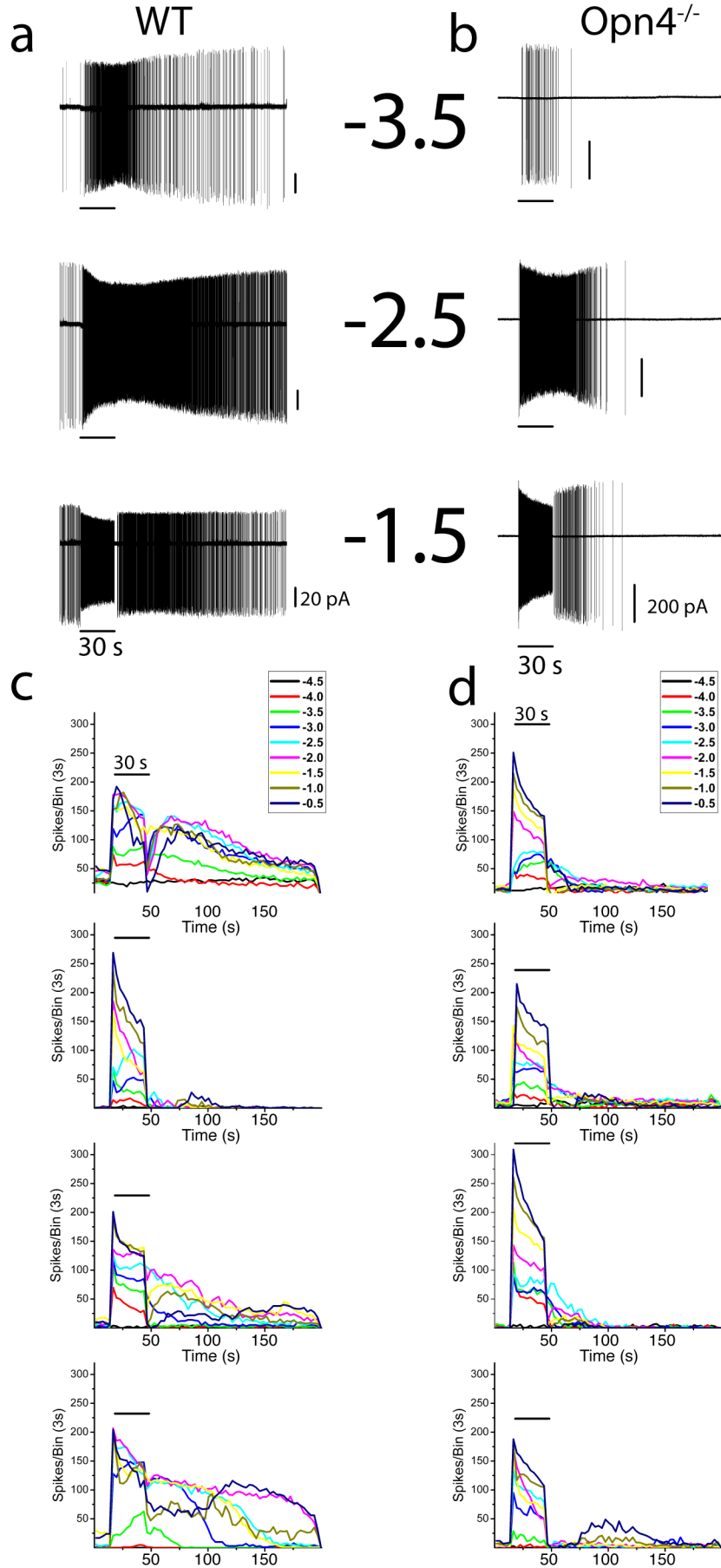
Supplementary Figures.....	2
Supplementary Experimental Procedures.....	6
References.....	17



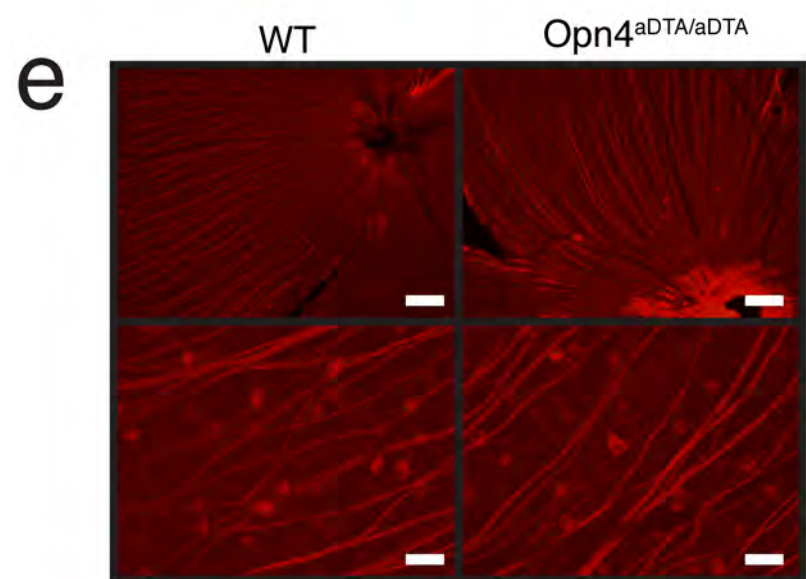
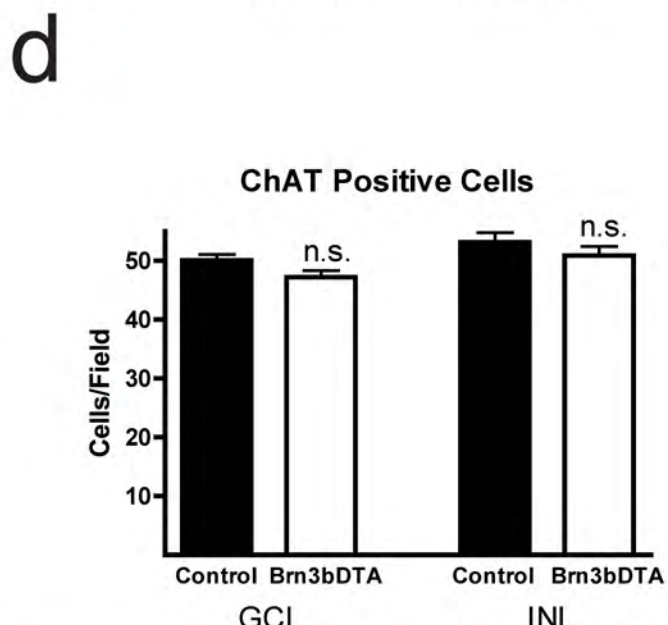
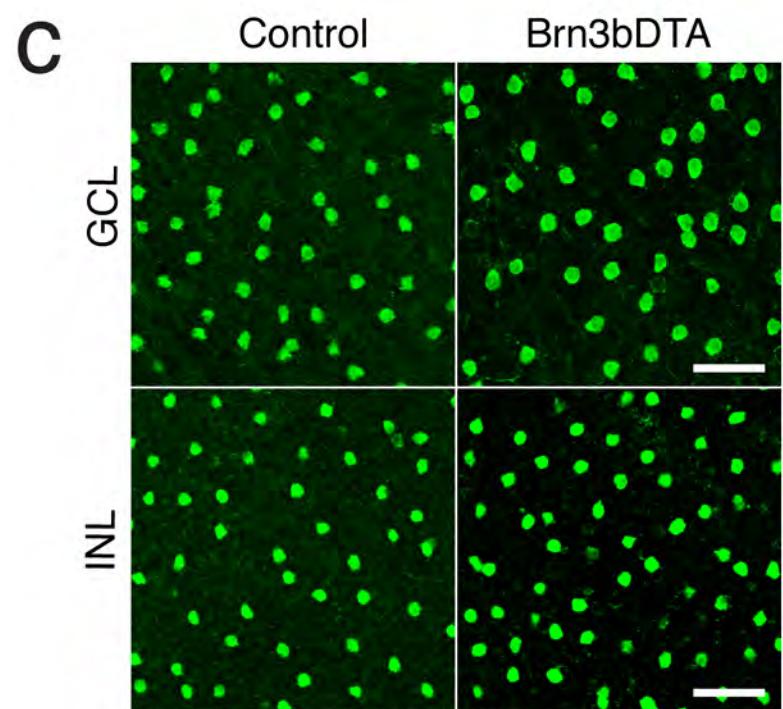
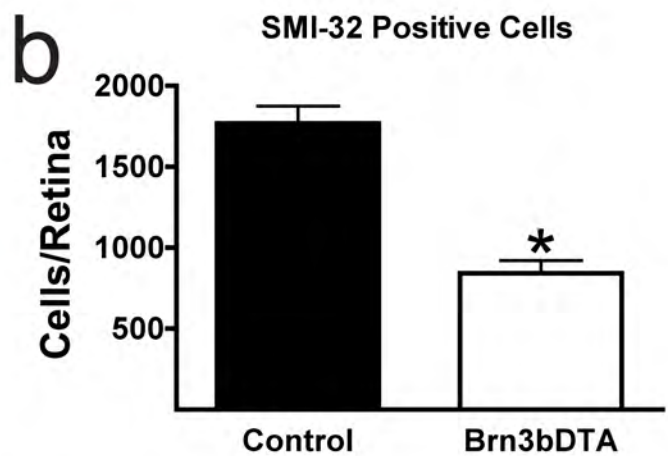
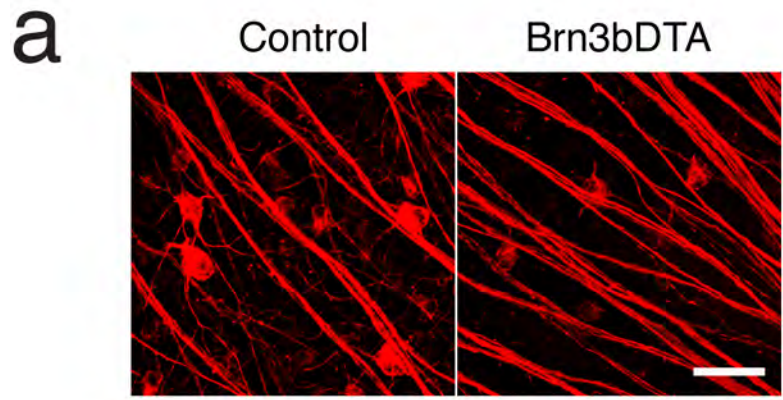
Supplemental Fig. 1 (Related to Fig. 1). Melanopsin immunostaining does not colocalize with SMI-32 immunostaining. Wholemount retinas from WT mice were stained with an antibody against (a) melanopsin and (b) SMI-32. (c) No overlap was observed between cells staining for melanopsin (yellow arrows) and SMI-32 (white arrows). Scale bar = 50 μ m.



Supplemental Fig. 2 (Related to Fig. 2). ON alpha-like RGCs in the ground squirrel are intrinsically photosensitive. (a) ON alpha-like cell from ground squirrel retina from panels d,e filled with Lucifer Yellow. Inset: Dendrites of cell ramify in S4/S5. ChAT bands are shown in purple. (b) Cell from d,e filled with Lucifer Yellow (green) costained with SMI-32 (red) and DAPI (blue). (c) Cell from d,e is positive for SMI-32 (red). DAPI is shown in blue. (d) Whole cell voltage clamp recording of response from cell in a-c. Inset shows transient component of rod/cone mediated light response. Lower panel shows expanded scale where intrinsic component is visible under control conditions. (e) Cell from d recorded in the presence of a cocktail of synaptic blockers at 50% (top trace) and 100% (bottom trace) of maximum intensity. In the absence of rod/cone signaling, cell responds with sluggish and sustained inward current. (f) Morphology of ON alpha-like RGCs recorded from ground squirrel retina ($n = 4$). (g) Amino acid sequence of ground squirrel (top) and mouse (bottom) melanopsin. Sequence of ground squirrel melanopsin was confirmed by PCR of genomic DNA exons and aligned to that of mouse. Melanopsin from the ground squirrel contains a functional open reading frame. The 7 transmembrane (TM1-7) domains for the mouse melanopsin protein are labeled (Provencio et al., 2000). The invertebrate-like tyrosine counterion (•), DRY domain (bracket), and Schiff's base lysine (*) are also indicated. Vertical lines between ground squirrel and mouse amino acid residues indicate identical amino acids, double dots indicate conserved substitutions, single dots indicate semi-conserved substitutions. (a) Scale bar is 20 μ m and 10 μ m for inset (b-c) Scale bar 10 μ m (f) Scale bar 50 μ m. All cells were stimulated with 30s, full-field, 480 nm stimulus. Horizontal bars indicate 30 s light stimulus. RGC: retinal ganglion cell. ChAT: choline acetyl transferase.



Supplemental Fig. 3 (Related to Fig. 3). ON alpha RGCs in WT and *Opn4*^{-/-} mice differentially encode irradiance following stimulus offset. (a,b) Raw data for extracellular recordings of WT (a) and *Opn4*^{-/-} (b) ON alpha RGC responses at increasing light intensities of -3.5, -2.5, and -1.5 LogI. (c,d) Spikes/3s Bin for WT (c) and *Opn4*^{-/-} (d) cells not shown in Fig. 4. Cell 2 in (c) was not included in further analyses. Horizontal scale bars (a-d) = 30 s. Vertical scale bars (a) = 20 pA, (b) = 200 pA. Legends indicate stimulus intensities (LogI). Full Intensity (0LogI) = 1.7×10^{16} photons/cm²/s.



Supplemental Fig. 4 (Related to Fig. 4). Alpha RGCs are reduced, but cholinergic amacrine cells are unaffected in Brn3bDTA mice while alpha RGCs are normal in *Opn4^{aDTA/aDTA}* mice.

(a) SMI-32 staining in control (*Opn4^{Cre/+}*) and Brn3bDTA (*Opn4^{Cre/+}, Brn3b^{zDTA/+}*) animals. Scale bars = 50 μ m (b) The total number of SMI-32 positive cells/retina is significantly reduced by approximately 50% in Brn3bDTA animals. (c) ChAT staining in control and Brn3bDTA animals in the GCL and INL. Scale bars = 50 μ m (d) No significant differences were observed in ChAT positive cell numbers between the two groups. (e) SMI-32 positive cells in *Opn4^{aDTA/aDTA}* mice ($N = 3$ mice, right panels) showed comparable distribution and morphology compared to WT (left panels). A retina from one *Opn4^{aDTA/aDTA}* mouse was reconstructed and the number of SMI-32 positive cells was comparable to WT (2148 cells), and we therefore did not quantify total numbers for the additional retinas. Scale bar top panels: 200 μ m, bottom panels: 50 μ m. Chat: choline acetyltransferase GCL: ganglion cell layer INL: inner nuclear layer.* $p < 0.05$, t-test. All values are Mean \pm SEM.

SUPPLEMENTAL EXPERIMENTAL PROCEDURES

Animals

For immunohistochemistry experiments, we used 1-3 month old mice from *Opn4^{Cre}* mice (Ecker et al., 2010) crossed with the Thy1-Brainbow 1.0 (referred to as Brainbow-1.0) reporter (Livet et al., 2007) line purchased from Jackson labs. This generates a mouse line (*Opn4^{Cre/+}*;Brainbow-1.0) in which all ipRGCs are labeled with cyan (CFP) and yellow (YFP) fluorescent proteins, referred to in the text as simply fluorescent proteins (FPs). For electrophysiological recordings, we used 25 to 50 day old C57/Bl6 WT mice or the previously described melanopsin knockout *Opn4^{LacZ/LacZ}* line (*Opn4^{-/-}*) (Hattar et al., 2002). All mouse lines used for behavior were on a mixed B6/129 background and have been backcrossed for at least ten generations. For OKR behavioral experiments, adult male and female at 2-6 months of age WT, *Opn4^{LacZ/LacZ}* (Hattar et al., 2002), *Opn4^{Cre/+}* (Ecker et al., 2010), *Opn4^{Cre/+}*; *Brn3b^{zDTA/+}* (Chen et al., 2011), or *Opn4^{aDTA/aDTA}* were used (Guler et al., 2008). For the visual water task (VWT), control mice were WT or *Opn4^{Cre/+}* mice. The contrast sensitivity of these mice was statistically similar and therefore their responses were grouped. *Opn4^{-/-}* mice in this task were *Opn4^{LacZ/LacZ}* or *Opn4^{Cre/Cre}* mice. All animals were handled in accordance with guidelines of the Animal Care and Use Committees of Johns Hopkins University, the University of Minnesota, the National Eye Institute or Cornell University.

Immunohistochemistry

Isolated retinas were fixed for 1 hour in 2% Ultra Pure paraformaldehyde (Electron Microscopy Sciences) in phosphate buffered saline (PBS). Retinas were then washed for 1 hour and placed in blocking solution of 0.3% Triton X-100 in PBS plus 6%

goat serum and 2% donkey serum overnight at 4°C. Retinas were then placed in blocking solution containing a monoclonal mouse antibody against the non-phosphorylated form of the neurofilament heavy chain polypeptide (SMI-32; 1:500, Covance) and sheep antibody to green fluorescent protein (GFP), which also recognizes CFP and YFP variants (Millipore; 1:500) for 2-3 days at 4°C. Retinas were then washed for 1 hour in PBS and placed in blocking solution plus a goat anti-mouse (gamma-1 subunit) antibody conjugated to AF-594 (1:500; Invitrogen) and a donkey anti-sheep antibody conjugated to AF-488 (1:500; Invitrogen). Retinas were then washed for 1 hour in PBS and mounted in Vectashield (Vector Labs). Images were taken on a Zeiss Axio Imager.M1 microscope. ChAT staining was performed as described above, but using a goat anti-ChAT antibody (1:250 Millipore) and donkey anti-goat secondary antibody (1:500 Invitrogen). Melanopsin immunostaining was performed essentially as described above, but using rabbit anti-melanopsin antibody (1:500; UF006, Advanced Targeting Systems) and incubated for 3-4 days in primary antibody solution and then washed overnight before placing retinas in secondary antibody solution containing a goat ant-rabbit antibody conjugated to AF-488 (1:500; Invitrogen).

For single cell filling in mouse, 0.3% Neurobiotin was included in the intracellular solution. After retraction of the electrode, the dye was allowed to diffuse for at least ten minutes. Retinas were then fixed in 4% paraformaldehyde for 1 hour, washed for 1 hour, and placed in the blocking solution described above overnight at 4°C. Retinas were then placed in a solution containing blocking solution plus Streptavidin (1:500; Vector Labs) conjugated to AF-488 (1:500) and the mouse anti-SMI-32 antibody (1:500) at room

temperature for 4-6 hours and then overnight at 4°C. Retinas were then washed for 1 hour and placed in a solution containing Streptavidin conjugated to AF-488 (1:500) and the goat anti-mouse (gamma-1 subunit) conjugated to AF-594 (1:500) for 3 hours at room temperature on a shaker. Retinas were then washed for 1 hour in PBS and mounted in Vectashield. Images for cell fills were performed on an upright Olympus Fluoview 1000 laser scanning confocal microscope (Olympus).

For single cell filling in squirrel, cells were filled with 1% Lucifer Yellow or 1% Neurobiotin and fixed for 20 minutes in 4% PFA. Tissues were processed as previously described (Li and DeVries, 2004). Briefly, after wash and blocked with 3% Donkey serum in 0.1M PB, tissues were incubated with primary antibodies for 3-5 days. The following antibodies were used: a rabbit anti-lucifer yellow antibody (1:100, Molecular Probes) a goat anti-ChAT antibody (1:100, Millipore), a mouse anti-SMI-32 antibody (1:500, Covance). After washing with 0.1M PB, tissues were incubated with secondary antibodies – donkey anti-goat Cy5, donkey anti-mouse Cy3, donkey anti-rabbit 488 or streptavidin conjugated 488 (all at 1:200), and 6 µM 4',6-diamidino-2-phenylindole (DAPI). Images were acquired with an LSM-510 confocal microscope (Zeiss) and edited with Zeiss Zen software and Photoshop CS4 (Adobe Systems). A 20x dry lens and a 63x oil immersion lens were used.

Image brightness and contrast was adjusted using Adobe Photoshop CS4, and morphological analysis was performed using Neurolucida (MicroBrightField). Coverage factors were calculated by taking the product of the spatial density of cells over the

entire retina (assumed to be 14mm²) by the dendritic field area calculated using that measured from Neurobiotin filled ON and OFF alpha RGCs (Berson et al., 2010).

Electrophysiology

Dissections were performed as described previously (Schmidt and Kofuji, 2011). Briefly, animals were killed by CO₂ asphyxiation and the eyes were enucleated in a dark room with minimal ambient light. Retinas were removed from eyecups under a standard dissection scope and placed in 95% O₂-5%CO₂ bicarbonate buffered Ames' solution (Sigma) at room temperature. Before recording, retinas were treated with Ames' solution containing collagenase/hyaluronidase (240 and 1000 U/ml, respectively) at room temperature for 5-10 min to remove vitreous. The flat-mount retina was viewed on a monitor using infrared illumination and a CCD camera. Cells in the ganglion cell layer with large diameter (≥ 20 um) somas were targeted for patch-clamp recordings. Signals were amplified using an Axon 700B Amplifier (Molecular Devices) with extracellular solution containing 95% O₂-5%CO₂ bicarbonate buffered Ames' solution at room temperature, which allowed for stable and robust light-evoked synaptic responses. Recordings were made with fire-polished borosilicate pipettes (3–7 MΩ; Sutter Instruments). For whole cell recordings, pipettes were filled with (in mM): 125 K-gluconate, 2 CaCl₂, 2 MgCl₂, 10 EGTA, 10 HEPES, 0.5 NaGTP, and 2 Na₂ATP, pH to 7.2, with KOH. Intracellular solutions also contained 10–20 μM Alexa Fluor-594 hydrazide (AF-594) (Invitrogen) and 0.3% Neurobiotin. Current and voltage acquisitions were performed with a Digidata 1322 D/A and A/D converter connected to a personal computer running pClamp 10 software (Molecular Devices). Liquid junction potentials

between the bath and electrode (14 mV) were calculated using the Liquid Junction Potential Calculator (pClamp 10) and were corrected offline in all recordings. Retinas were allowed to dark adapt for 5 min before the first light stimulus, and any stimuli were placed 5 min apart to allow the cell membrane potential to return completely to baseline.

Extracellular loose patch and cell attached experiments were made as described previously (Schmidt and Kofuji, 2010). Briefly, loose patch recordings were performed by obtaining a 100–700 M Ω seal and recording in voltage-clamp mode with a holding potential of 0 mV. Cell-attached recordings were performed by obtaining a \geq 1 G Ω seal and recording in voltage-clamp mode with a holding current equal to that of the membrane potential (Perkins, 2006). Pipette solution consisted of (in mm) 150 NaCl, 10 HEPES, pH 7.4. Only ON cells with a sustained synaptic response similar to that observed for the ON alpha cells encountered in the whole cell recordings were used for further analysis in these experiments.

Extracellular recordings were analyzed off-line with Clampfit (Molecular Devices). Whole cell recordings were analyzed with Igor Pro 6.0, and membrane potential values were measured from raw traces over a 1 s sliding time window to maximize the signal-to-noise ratio. Series resistance was noted in all recordings, but uncompensated. Light responses were defined as the maximum depolarization of the averaged trace during the light stimulus. For kinetics measurements, rise time (RT) was defined as the time for the cell membrane potential or whole-cell current to go from 10 to 90% of maximum, and decay time (DT) was defined as the time for recording to decline to 37% of the maximum value following light offset. Light stimuli for all experiments were full-field,

band-pass filtered 480 nm light of 1.66×10^{16} photons · cm²/s¹ delivered using a xenon lamp feeding the camera port. The field of the stimulus was sufficiently large to encompass the entire dendritic arbor, and the focal plane of the stimulus was in the ganglion cell layer. A filter wheel fitted with various neutral-density filters (Chroma Technologies) and shutter (Lambda-3, Sutter Instruments) was used to control the intensity and duration of light stimuli. For single intensity experiments, stimuli were delivered at -1LogI. Irradiance measurements were made with a calibrated radiometer model S370 (UDT Instruments). Irradiance-response experiments were performed as described previously (Schmidt and Kofuji, 2009). In irradiance response experiments, cells were stimulated with full-field 480 nm light while neutral density filters were interposed in the light path resulting in stimulation intensities of -4.5 to -0.5LogI (increasing in intensity by 0.5LogI/stimulation) with at least 3 minutes in between stimulations. Spike frequencies at -4.5LogI (which were always subthreshold when the tissue was partially light adapted) were treated as baseline spike rates, and subtracted from values for subsequent stimuli in analysis of irradiance response experiments. Total spikes were measured in three time windows: during the 30s light stimulus, from 0 to 60s following light offset, and from 60 to 120s following light offset. For light step experiments, light stimuli were 1 minute in duration and presented in the following order with no intervening darkness: Dark, -4.5LogI, -3.0LogI, -2.5LogI, -2.0LogI, -1.5LogI, -1.0LogI, -1.5LogI, -2.0LogI, -2.5LogI, -3.0LogI, -4.5LogI, Dark. Spike frequency plots were generated by counting the number of spikes in 3s bins. For dim light recordings, animals were dark adapted overnight and retinas were dissected in dim red light.

Putative alpha RGCs were selected under infrared optics based on soma size and were verified to have an ON sustained synaptic response to a 1s flash of 480 nm light. Cells were then allowed 10 minutes to re-dark adapt and were perfused with a cocktail of synaptic blockers (see Pharmacology section). Cells were then stimulated for 5 minutes with light at 5.3×10^{11} photons/cm²/s. Cells were then stimulated with bright (5.3×10^{13} photons/cm²/s) light.

Dissections and electrophysiology in ground squirrel was performed as described previously (Chen and Li, 2012; Schmidt and Kofuji, 2010). Intracellular solution contained, in mM: KGluconate, 99; KCl, 32; MgCl₂, 4.5; HEPES 10; tetrapotassium BAPTA (Molecular Probes), 5; ATP, 3; GTP 1; and Neurobiotin (Vector Laboratories), 0.1. pH was adjusted to 7.4 with KOH.. Light stimulus was full field 480 nm light at intensity of 1.94×10^{16} photons/cm²/s. Data were collected and analyzed using Igor Pro. Recordings were obtained with Axopatch 200B amplifiers (Molecular Devices), and currents low-pass filtered at 1 or 5 kHz using the 4 pole Bessel filter on the amplifier. Data were digitized at 10 kHz using an ITC-18 interface (HEKA) controlled by a Dell computer running IgorPro 6.0 (WaveMetrics). Data were analyzed with custom-made software (IgorPro 6.0).

Statistical analyses were performed using Origin 7.5 (MicroCal) or GraphPad Prism . Statistical comparison of means was performed using a Student's *t* test or one-way ANOVA with Tukey's *post hoc* test or a Mann-Whitney U test and significance was concluded when $p < 0.05$. Data are presented as mean \pm SE.

Pharmacology

Synaptic blocker solution used to measure intrinsic photosensitivity included: 250 μ M DL-2-Amino-4-phosphonobutyric acid (DL-AP4, a GroupIII metabotropic glutamate receptor (mGluR) agonist that selectively silences the ON pathway (Slaughter and Miller, 1981)(Tocris)), 10 μ M 2,3-Dioxo-6-nitro-1,2,3,4-tetrahydrobenzo[*f*]quinoxaline-7-sulfonamide (NBQX, an α -amino-3-hydroxy-5-methyl-4-isoxazolepropionic acid (AMPA) receptor antagonist)(Tocris), 20 μ M 6-Cyano-7-nitroquinoxaline-2,3-dione (CNQX, an AMPA/Kainate receptor antagonist)(Tocris), 60 μ M DL-2-Amino-5-phosphopentanoic acid (DL-APV, an *N*-Methyl-D-aspartic acid (NMDA) receptor antagonist)(Tocris), 50 μ M picrotoxin (a γ -Aminobutyric acid (GABA) A receptor antagonist)(Sigma), and 5 μ M strychnine (a glycine receptor antagonist)(Sigma). Cells were bathed in synaptic blocker cocktail for at least 5 minutes prior to light stimulation. For squirrel recordings, synaptic blocker cocktail consisted of: 4 μ M L-AP4, 10 μ M NBQX, 60 μ M D-APV, 50 μ M picrotoxin, 5 μ M strychnine.

Sequence of ground squirrel melanopsin

PCR primers were designed based on the Ensemble Genomic Database to each exon of the ground squirrel melanopsin gene and then sequenced. The cDNA sequence obtained matched that of the Ensemble database and the amino acid sequence was then aligned to that of mouse.

Optokinetic Tracking (OKT) in a Virtual Optokinetic System (VOS)

A vertical sine wave grating was projected as a virtual cylinder in 3D coordinate space on computer monitors (54 Lux) arranged in a quadrangle around a testing arena (Prusky et al., 2004); OptoMotry \circledcirc , CerebralMechanics, Lethbridge, Alberta).

Unrestrained animals were placed individually on an elevated platform at the epicenter of the arena. An experimenter used a video image of the arena from above to view the animal, and followed the position of its head in real time with the aid of a computer mouse and a crosshair superimposed on the video frame. The X-Y positional coordinates of the crosshair centered the hub of the cylinder, enabling the wall to be maintained at a constant 'distance' from the animal's eyes, thereby fixing the spatial frequency (SF) of the stimulus. When the cylinder was rotated and the animal followed with head and neck movements that tracked the rotation, it was judged that the animal's visual system could distinguish the grating.

Assessment of OKT Spatial Frequency and Contrast Thresholds

Homogeneous gray was projected on the cylinder at the beginning of each testing session. For the measurement of SF thresholds, the experimenter waited until the animal was still, at which time gray was replaced with a low spatial frequency (0.04-0.10 cycles/degree (c/d)), high contrast sine wave grating of the same mean luminance, drifting in one direction. The animal was assessed for tracking behavior for a few seconds, and then the gray stimulus was restored. This procedure was repeated until unambiguous examples of tracking were observed. The SF of the grating was then systematically changed, with multiple tests at each SF, until the animal no longer tracked. The process was repeated at least three times until the highest SF that elicited tracking was established. Occasional clicking noises or finger taps on the apparatus were used to induce animals to change their position, or to stop moving, both of which facilitated more rapid testing. Thresholds through each eye were measured

independently by altering the direction of cylinder rotation, since only temporal-to-nasal stimulus movement in the visual field evokes tracking (Douglas et al., 2005). All experiments were conducted using a cylinder rotation rate of 12°/sec, which is the most favorable cylinder velocity to generate OKT across varying SFs.

Contrast thresholds were identified using similar procedures, except that testing began with a grating of maximum (~100%) contrast, which was then systematically changed until the minimum contrast to elicit tracking was identified. Thresholds were measured at 6 spatial frequencies (0.031, 0.064, 0.092, 0.103, 0.192, 0.272 c/d), and a contrast sensitivity function was generated by calculating a Michelson contrast using the screen luminances $(\text{max}-\text{min})/(\text{max}+\text{min})$ and plotting the reciprocal of the threshold. Measurements were made at 54, 4, and 2 Lux (calibrated photodiode; United Detector Technologies, San Diego, CA) after dark adaptation for a minimum of 2 hours). Extraneous sources of light in the testing arena were eliminated, neutral density (ND) filters (Lee Filters USA) were placed over the stimulus screens, and testing was conducted with an infrared-sensitive camera under infrared illumination.

All testing was conducted during the daylight circadian cycle, and a complete set of SF and contrast thresholds for an animal through each eye (14 in total) were generated in 10-15 minutes. Experimenters were blind to an animal's experimental condition and previously recorded thresholds, and adjunct observers were used to validate threshold assessments.

Visual Water Task

The visual water task was performed essentially as described previously (Prusky et al., 2004; Prusky et al., 2000). Briefly, animals were trained in a swimming task to choose one of two arms of a Y-shaped maze, a sine wave grating at 100% contrast over a stimulus at 50% gray. The correct side contained a hidden platform allowing the mouse to escape the water. Once mice regularly achieved 95-100% success, animals were tested with stimuli of decreasing contrasts decreasing at 10% (at higher contrasts), 5%, or 1% (at lower contrasts) intervals. Animals were determined to be able to detect the stimulus when they achieved 4 correct in a row or 7/10 trials correct. Once animals missed a given stimulus twice but got at least 7/10 on two separate trials at the next highest contrast, this was determined as the animal's contrast threshold. Sine wave stimuli were generated using MatLab and then printed on a Canon Pro9000 Mark II printer and laminated with a matte finish. All testing was performed under room light at 155 lux. Performance was assessed impartially using AnyMaze software (Stoelting Co.). Contrast thresholds were tested at 0.089 cycles/degree.

REFERENCES

- Berson, D.M., Castrucci, A.M., and Provencio, I. (2010). Morphology and mosaics of melanopsin-expressing retinal ganglion cell types in mice. *J Comp Neurol* 518, 2405-2422.
- Chen, S., and Li, W. (2012). A color-coding amacrine cell may provide a blue-Off signal in a mammalian retina. *Nat Neurosci* 15, 954-956.
- Chen, S.K., Badea, T.C., and Hattar, S. (2011). Photoentrainment and pupillary light reflex are mediated by distinct populations of ipRGCs. *Nature* 476, 92-95.
- Douglas, R.M., Alam, N.M., Silver, B.D., McGill, T.J., Tschetter, W.W., and Prusky, G.T. (2005). Independent visual threshold measurements in the two eyes of freely moving rats and mice using a virtual-reality optokinetic system. *Vis Neurosci* 22, 677-684.
- Ecker, J.L., Dumitrescu, O.N., Wong, K.Y., Alam, N.M., Chen, S.K., LeGates, T., Renna, J.M., Prusky, G.T., Berson, D.M., and Hattar, S. (2010). Melanopsin-expressing retinal ganglion-cell photoreceptors: cellular diversity and role in pattern vision. *Neuron* 67, 49-60.
- Guler, A.D., Ecker, J.L., Lall, G.S., Haq, S., Altimus, C.M., Liao, H.W., Barnard, A.R., Cahill, H., Badea, T.C., Zhao, H., *et al.* (2008). Melanopsin cells are the principal conduits for rod-cone input to non-image-forming vision. *Nature* 453, 102-105.
- Hattar, S., Liao, H.W., Takao, M., Berson, D.M., and Yau, K.W. (2002). Melanopsin-containing retinal ganglion cells: architecture, projections, and intrinsic photosensitivity. *Science* 295, 1065-1070.
- Li, W., and DeVries, S.H. (2004). Separate blue and green cone networks in the mammalian retina. *Nat Neurosci* 7, 751-756.

- Livet, J., Weissman, T.A., Kang, H., Draft, R.W., Lu, J., Bennis, R.A., Sanes, J.R., and Lichtman, J.W. (2007). Transgenic strategies for combinatorial expression of fluorescent proteins in the nervous system. *Nature* *450*, 56-62.
- Perkins, K.L. (2006). Cell-attached voltage-clamp and current-clamp recording and stimulation techniques in brain slices. *J Neurosci Methods* *154*, 1-18.
- Provencio, I., Rodriguez, I.R., Jiang, G., Hayes, W.P., Moreira, E.F., and Rollag, M.D. (2000). A novel human opsin in the inner retina. *J Neurosci* *20*, 600-605.
- Prusky, G.T., Alam, N.M., Beekman, S., and Douglas, R.M. (2004). Rapid quantification of adult and developing mouse spatial vision using a virtual optomotor system. *Invest Ophthalmol Vis Sci* *45*, 4611-4616.
- Prusky, G.T., West, P.W., and Douglas, R.M. (2000). Behavioral assessment of visual acuity in mice and rats. *Vision Res* *40*, 2201-2209.
- Schmidt, T.M., and Kofuji, P. (2009). Functional and morphological differences among intrinsically photosensitive retinal ganglion cells. *J Neurosci* *29*, 476-482.
- Schmidt, T.M., and Kofuji, P. (2010). Differential cone pathway influence on intrinsically photosensitive retinal ganglion cell subtypes. *J Neurosci* *30*, 16262-16271.
- Schmidt, T.M., and Kofuji, P. (2011). An isolated retinal preparation to record light response from genetically labeled retinal ganglion cells. *J Vis Exp*.
- Slaughter, M.M., and Miller, R.F. (1981). 2-amino-4-phosphonobutyric acid: a new pharmacological tool for retina research. *Science* *211*, 182-185.